Tuning the resistive switching in tantalum oxide-based memristors by annealing

Li, Yang; Suyolcu, Y. Eren; Sanna, Simone; Christensen, Dennis Valbjørn; Traulsen, Marie Lund; Stamate, Eugen; Pedersen, Christian Søndergaard; van Aken, Peter A.; García Lastra, Juan Maria; Esposito, Vincenzo

Total number of authors:
11

[Link back to DTU Orbit]

Tuning the resistive switching in tantalum oxide-based memristors by annealing

Yang Li ⓘ, Y. Eren Suyolcu ⓘ, Simone Sanna ⓘ, Dennis Valbjørn Christensen ⓘ, Marie Lund Traulsen ⓘ, Eugen Stamate ⓘ, Christian Søndergaard Pedersen ⓘ, Peter A. van Aken ⓘ, Juan Maria García Lastra ⓘ, Vincenzo Esposito ⓘ, and Nini Pryds ⓘ

COLLECTIONS

Paper published as part of the special topic on Chemical Physics, Energy, Fluids and Plasmas, Materials Science and Mathematical Physics

View Online   Export Citation   CrossMark

ARTICLES YOU MAY BE INTERESTED IN

Tuning the resistive switching in tantalum oxide-based memristors by annealing

View Online   Export Citation   CrossMark

Yang Li,[1]   Y. Eren Suyolcu,[2,3]   Simone Sanna,[1,4]   Dennis Valbjørn Christensen,[1]   Marie Lund Traulsen,[1]
Eugen Stamate,[1]   Christian Søndergaard Pedersen,[1]   Peter A. van Aken,[2]   Juan Maria García Lastra,[1]
Vincenzo Esposito,[1]   and   Nini Pryds[1,a]

AFFILIATIONS

[1] Department of Energy Conversion and Storage, Technical University of Denmark, Lyngby 2800, Denmark
[2] Max Planck Institute for Solid State Research, Heisenbergstraße 1, Stuttgart 70569, Germany
[3] Department of Materials Science and Engineering, Cornell University, Ithaca, New York 14853, USA
[4] Dipartimento di Ingegneria Civile e Ingegneria Informatica and CNR-SPIN, Università di Roma Tor Vergata, Via del Politecnico 1, I-00133 Roma, Italy

[a] Author to whom correspondence should be addressed: nipr@dtu.dk

ABSTRACT

A key step in engineering resistive switching is the ability to control the device switching behavior. Here, we investigate the possibility to tune the resistive switching of tantalum oxide (TaO_x)-based memristors from a non-switchable state to a switchable state by applying post-fabrication annealing of the devices. The switching of the devices was found to be related to: (1) the oxidation state changes in the TaO_x thin film after annealing and (2) the local variations in oxygen stoichiometry in the vicinity of the interface between the TiN electrode and the TaO_x active resistive layer. We further discuss the possible mechanism behind the resistive switching after annealing. This experimental approach provides a simple but powerful pathway to trigger the resistive switching in devices that do not show any resistive switching initially.

I. INTRODUCTION

Tantalum oxide (TaO_x) is widely used as a resistive switching material in memristors as it exhibits excellent features such as superior endurance of more than 10^{12} cycles[1] and ultra-fast switching speed of sub-nanoseconds.[2] Tantalum oxide is a complex system that includes more than 20 non-equilibrium phases and two equilibrium Ta_2O_5 (tantalum pentoxide) phases.[3] Being able to control these phases is an essential step in achieving highly controllable resistive switching behaviors in tantalum oxide memristors.

Two simple but effective methods that enable to tune and control the tantalum oxide (TaO_x)-based memristor behaviors are: (1) manipulating the TaO_x thin film growth conditions[4–7] or/and (2) annealing the TaO_x thin film after deposition.[8–10] We have shown in our previous work[4] that we can fine tune and control the resistivity of the TaO_x thin film during the growth by pulsed laser deposition

(PLD). By varying the oxygen pressure during deposition from 10^{-6} to 2×10^{-2} mbar, the resistivity of the deposited tantalum oxide can be altered by more than six orders of magnitude as a result of a controlled oxygen stoichiometry. This, in turn, led to different resistive switching behaviors of the memristors. Memristors with TaO_x deposited at low oxygen pressure below and equal to 2×10^{-3} mbar showed no resistive switching, whereas TaO_x deposited at oxygen pressures above 2×10^{-3} mbar showed a resistive switching character.

Besides varying the oxygen pressure during thin film deposition, the annealing temperature is another critical factor influencing TaO_x phases. For example, a Ta_2O_5 pellet after been sintered at 1400–1600 °C for 24 h shows a monoclinic to orthorhombic phase transition by Raman scattering at about 327 °C.[11] Ta_2O_5 in an amorphous state (a-Ta_2O_5) transfer into low-temperature (LT) crystalline state (orthorhombic β-phase) at approximately 650 °C.

The orthorhombic β-phase can reversibly transfer into the high temperature (HT) crystalline tetragonal α-phase at approximately $1320 \pm 20\,°C$.[3,11,12]

Besides controlling the Ta_2O_5 phases by annealing at different temperatures, annealing in different gas atmospheres at elevated temperatures can also be an effective way to tune the stoichiometry of tantalum oxide.[8,10] This approach is also often used to further improve the mechanical, electrical, or optical properties of thin films by structural relaxation and stoichiometry change.[13,14]

Altogether, post annealing is an effective way to tune the properties of TaO_x-based memristors.[8,15,16] For example, annealing a TaO_x-based memristor in an oxygen atmosphere at $300\,°C$ can affect the oxygen stoichiometry, which has been found to improve the device endurance.[8] Annealing in NH_3 at $400\,°C$, on the other hand, resulted in the incorporation of hydrogen (H) species into TaO_x,[10] which improved the device endurance, lowered the forming voltage, and enhanced the retention lifetime of the formed conductive filaments. Besides the effect of annealing on the active TaO_x layer, the electrode materials may also be affected by the annealing process. For example, Raman scattering spectra indicated the presence of rutile TiO_2 signals in 1 μm thick TiN after annealing in air at $500\,°C$ for 2 h.[17]

So far, annealing of TaO_x-based memristors have been carried out on TaO_x films deposited either by sputtering or by atomic layer deposition (ALD). No systematic work on the effect of post-deposition annealing on the resistive switching behavior of TaO_x films fabricated by PLD has so far been reported. PLD is a powerful technique for the fabrication of complex oxide while preserving the stoichiometry. In this work, we focus on utilizing post-deposition annealing to tune the stoichiometry and resistive switching behaviors of tantalum oxide-based memristors. By using isochronal annealing steps imposed with controlled heating and cooling, we successfully trigger the switching behavior in devices, which did not show any switching initially. We also reveal the stoichiometry change of TaO_x after annealing and propose a possible mechanism for the triggering of the switching behavior.

II. EXPERIMENT

The configuration of the device film stack used in this study was $Si/SiO_2/TiN/TaO_x/W$ with TiN and W serving as the electrodes and TaO_x being the active memristive layer. The substrates are commercially available (100) silicon substrates with 100 ± 10 nm native silicon dioxide, and 100 nm TiN film on top (Prime Wafers), labeled as $Si/SiO_2/TiN$ substrates. The TiN layer in the $Si/SiO_2/TiN$ substrate acts as the bottom electrode. An active oxide layer of TaO_x thin films was deposited by pulsed laser deposition (PLD) through a square-shaped shadow mask in order to expose the TiN bottom electrode. A KrF excimer laser (248 nm, 10 Hz, 4 J/cm²) was used to ablate a commercial ceramic target of Ta_2O_5 (American Elements) with 99.99% purity and dimensions of 25.4 mm in diameter and 6 mm in thickness. The deposition was carried out keeping the target–substrate distance constant at 7.5 cm. The TaO_x thin films were deposited with a thickness of approximately 20 nm at room temperature (RT) with an oxygen pressure $P_{O2} = 2 \times 10^{-3}$ mbar inside the chamber. The tungsten (W) top electrode layer was deposited by DC magnetron sputtering without intentional substrate heating using the following parameters: 40 sccm Ar gas, 10^{-2} Torr deposition pressure, 320 V discharge voltage, and 0.2 A discharge current for a deposition time of 300 s. The W top electrodes were patterned into a circular shape with a diameter of 50 μm and a thickness of about 150 nm using an Al_2O_3 shadow mask.

All electrical tests were carried out using Keithley 4200A with an Imina probe station providing the contact to the W and TiN electrodes through W needle probes. During the two-terminal electrical tests, voltages were applied to the W top electrodes, and the TiN bottom electrodes were grounded. The voltage ramp with 10 mV per step was used in both SET and RESET processes. A compliance current of 1 mA was used in the SET process. The initial resistances of the devices follow a log-normal distribution, which means the log of the initial resistances follow normal distribution. In Fig. 1, the mean values are of the log of the initial resistances and the error bars are the standard deviations of the mean. The electrical conductivity
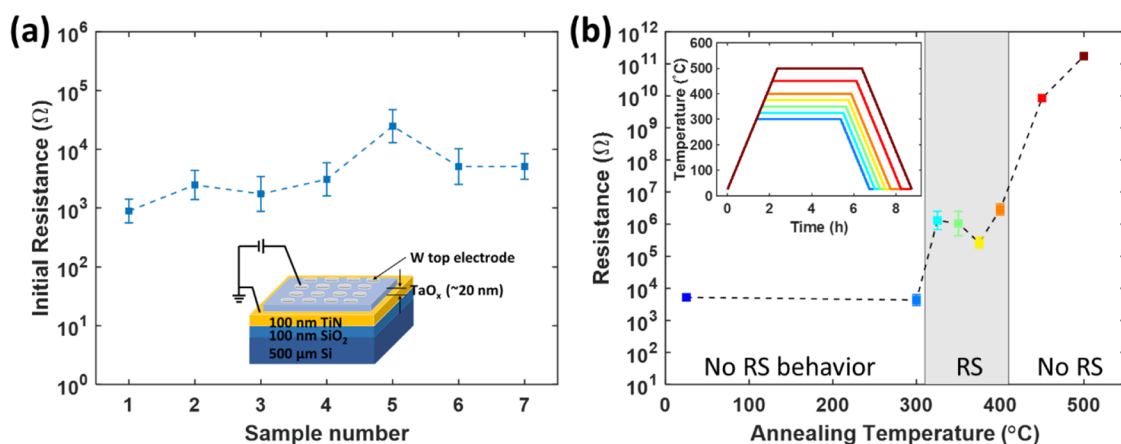
FIG. 1. (a) Initial resistance distribution for seven as-fabricated samples. Each sample contains 16 devices. The diameter of the top electrodes is 50 μm. The thickness of the TaO_x layer is about 20 nm. The inset in (a) shows a schematic illustration of the devices under test and the two-terminal electrical test setups. (b) Change in resistances after the annealing process at different temperatures. The inset in (b) shows the temperature profile during the annealing process. RS stands for resistive switching. The error bars represent the standard deviation of the mean.

was measured on rectangular-shaped samples (1×1 cm^2) in a van der Pauw configuration. A short description of the electrical measurement setup is described in the supplementary material (Figs. S1 and S2).

Chemical and structural changes in the materials induced by the annealing were characterized by x-ray photoelectron spectroscopy (XPS), x-ray diffraction (XRD), scanning transmission electron microscopy (STEM), and energy-dispersive x-ray spectroscopy (EDX). The XPS analyses were performed on an ESCALAB XI$^+$ x-ray photoelectron spectrometer (Thermo Fisher Scientific, East Grinstead, UK) using a monochromatic Al-Kα x-ray source with a 650 μm spot size and a take-off angle of 90° from the surface plane. A combined ion/electron gun (i.e., a dual-beam source) was used to control sample charging. The pressure in the analysis chamber was 4×10^{-8} mbar. High resolution local binding energy spectra were obtained for Ta-4f using 20 eV detector pass energy, a dwelling time of 50 ms, and an energy step size of 0.05 eV. The sputter depth profiling was performed on a fraction of the area of 0.7×0.7 mm^2 with monatomic Ar$^+$ ion beam. The beam has a kinetic energy of 3 KeV, for 10 s each level, and with 30 levels in total. All spectra were shifted according to the O1s spectra peak position using the second O1s spectrum of the as-deposited sample. For the XRD analysis, Bruker D8 Advanced diffractometer (Germany) with Cu K$_\alpha$ ($\lambda = 1.5406$ Å) radiation was used. For the STEM analyses, a probe-aberration corrected JEOL JEM-ARM200F microscope equipped with a cold field-emission electron source, a probe Cs-corrector (DCOR, CEOS GmbH), and a large solid-angle JEOL Centurio SDD-type EDX detector was used. STEM imaging and EDX analyses were performed at probe semi-convergence angles of 20 mrad and 28 mrad, resulting in probe sizes of 0.8 Å and 1.0 Å, respectively. Collection angles for high-angle annular dark-field (HAADF) images were 75–310 mrad.

III. RESULTS AND DISCUSSION

A set of seven samples were fabricated under the same conditions as described in the experimental part. Each sample contains 16 devices defined by a circular W top-electrode with a diameter of 50 μm and a 20 nm active TaO$_x$ layer. A schematic illustration of the device is shown in the inset of Fig. 1(a). Initially, all devices showed no resistive switching with an average low initial resistance of approximately 5.26 kΩ [Fig. 1(a)]. We annealed the samples at different temperatures ranging from 300 °C to 500 °C in air. Seven annealing temperatures were used: 300 °C, 325 °C, 350 °C, 375 °C, 400 °C, 450 °C, and 500 °C, with a fixed annealing time of 4 h and a ramping rate of 200 °C/h during heating and cooling [inset of Fig. 1(b)]. The resistances after the annealing process at different temperatures are shown in Fig. 1(b). After the annealing process, the ability of the samples to resistive switch was tested at room temperature.

The results of the annealing revealed the following: (1) For annealing temperature smaller than or equal to 300 °C, no resistive switching was observed inside the devices [Figs. 2(a) and 2(b)], (2) from 325 °C to 400 °C, the resistive switching was triggered [Figs. 2(c)–2(f)], and (3) above 400 °C, the average resistance of devices exceeds 10^{10} Ω, showing an insulating state with no resistive switching [Figs. 2(g) and 2(h)]. Typical *IV* curves and resistance distributions of the switching devices are shown in the supplementary material, Fig. S3.

Thus, only in a limited window, between 325 °C and 400 °C, we could trigger resistive switching behaviors in TiN/TaO$_x$/W structured devices. In the following, we, therefore, investigate the underlying origins responsible for enabling the resistive switching within this window and the reasons for terminating the resistive switching when annealed outside this window.
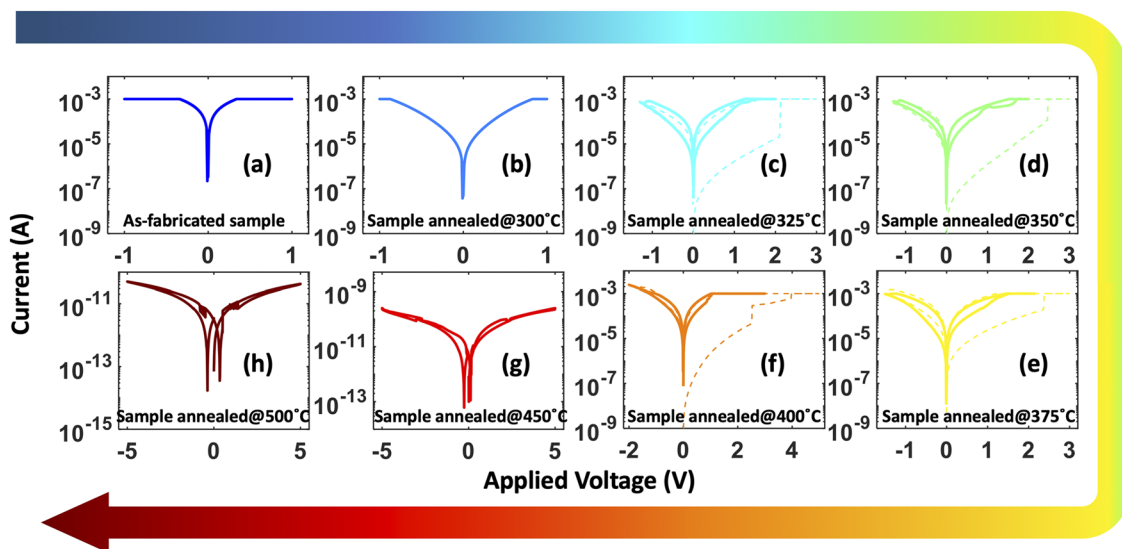

FIG. 2. Typical IV relation for (a) the as-fabricated devices, and (b)–(h) devices after annealed at 300 °C, 325 °C, 350 °C, 375 °C, 400 °C, 450 °C, and 500 °C, respectively. The dashed lines in (c)–(f) represent the corresponding forming and the first RESET processes.
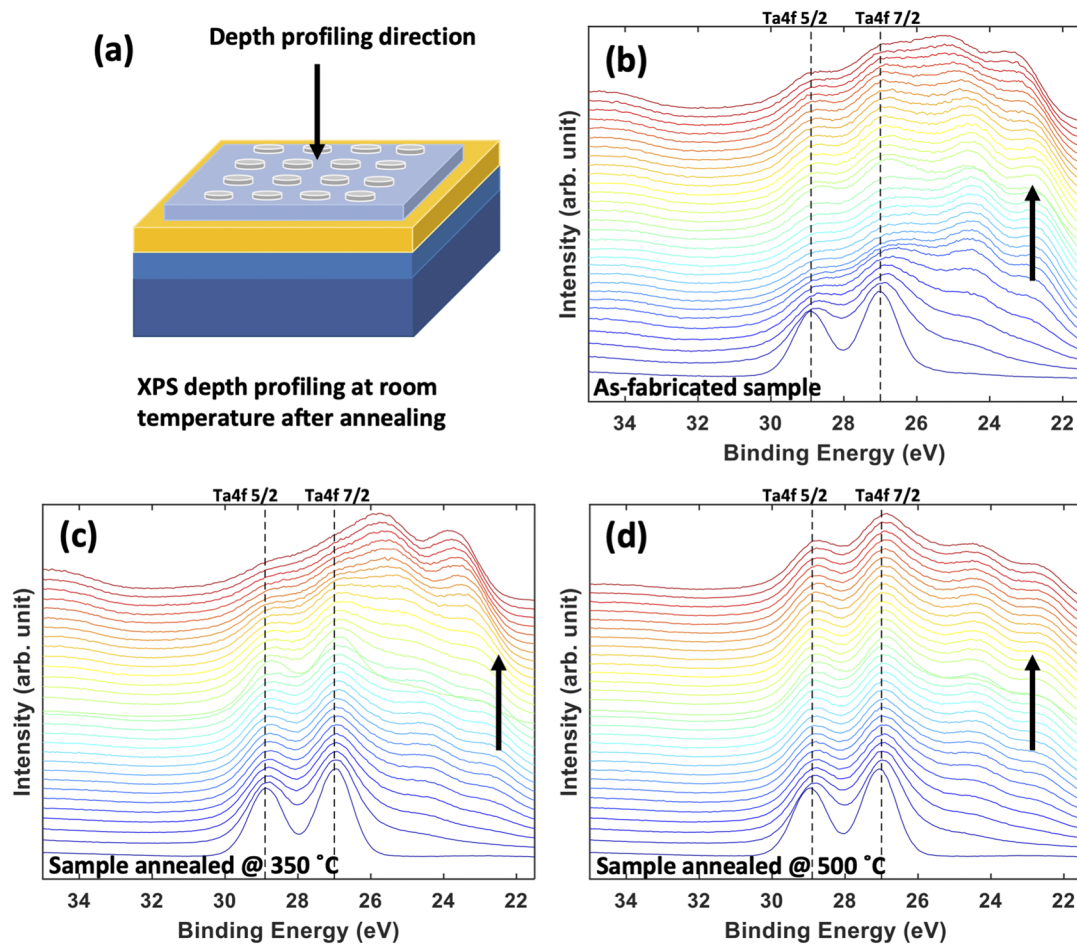
FIG. 3. (a) An illustration of the XPS depth profiling direction. XPS depth profiles of devices (b) as-fabricated, (c) after annealed at 350 °C, and (d) after annealed at 500 °C. The black arrows indicate the etching direction from the surface of TaO_x to the inner part of the TaO_x thin film. The dashed lines represent the binding energy for Ta^{5+}.

A. Oxidation and crystallinity of the TaO_x resistive switching layer

In order to understand the oxidation state and the stoichiometry of film and their relation to the resistive switching, we have studied three samples: (1) the as-fabricated sample, (2) the sample annealed at 350 °C, and (3) the sample annealed at 500 °C, by XPS depth profiling (Fig. 3). The black arrows in Fig. 3 represent the XPS depth profile direction from the surface of the TaO_x to the inner part of the TaO_x. The depth profiles taken from these samples have a similar analysis time, i.e., approximately a similar depth length.

The spectra were peak fitted using the CasaXPS software. All six oxidation states of Ta, i.e., Ta^{5+}, Ta^{4+}, Ta^{3+}, Ta^{2+}, Ta^{1+}, and Ta^{0}, were used to build the peak model for fitting. The details of the information of the fitting are given in Table S1 and Fig. S4 in the supplementary material. From the analysis, we can conclude that the TaO_x films contain a mixture of different oxidation states of tantalum. Figure 4 shows the results of the analysis where the O/Ta ratio of the three samples is plotted. As seen from this
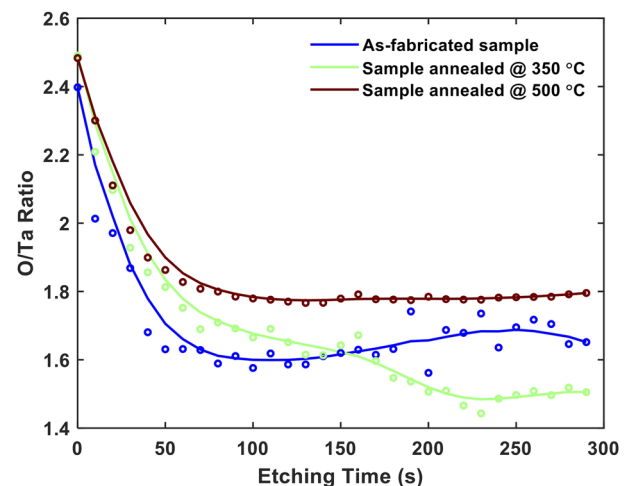

FIG. 4. The O/Ta ratio of the TaO_x films as a function of the etching time for all three samples under different annealing conditions.
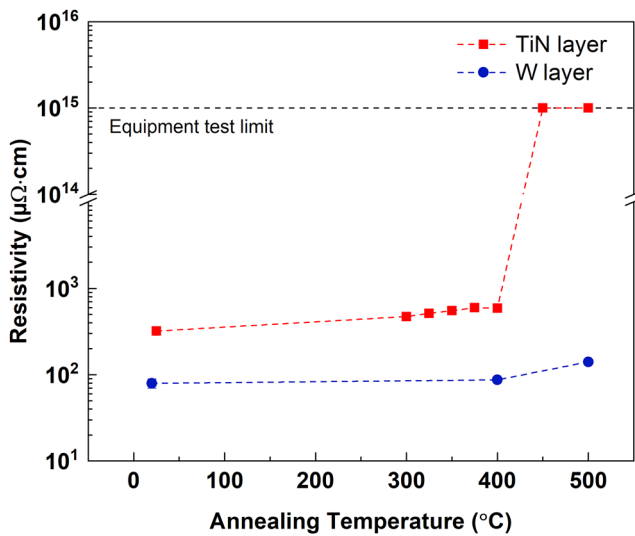
FIG. 5. Resistivity change of TiN and W layers after annealing at different temperatures. The resistivity was tested by using a four-probe van der Pauw configuration on 1×1 cm^2 samples.

figure, the oxygen content of the film increases as the annealing temperature increases for etching time up to about 150 s. For etching time larger than 150 s, for sample annealed at 350 °C, the oxygen content is lower than the as-fabricated sample, whereas the sample annealed at 500 °C shows the highest oxygen content above 150 s. These results indicate that after annealing at 350 °C, the TaO$_x$ is probably partially reduced causing the partial oxidation of the TiN layer.

By comparing the XPS results to the corresponding resistive switching of the heat-treated devices, the following picture emerged:

At annealing temperatures between 325 °C and 400 °C, a reaction between the TiN and TaO$_x$ takes place leading to the partial oxidation of TiN (TiON) and partial reduction of the TaO$_x$. This corresponds well with the XPS results (Fig. 4) and the resistive switching shown in Figs. 1 and 2. However, we cannot exclude that part of the contribution to the resistive switching might come from the possible formation of the TiON phase. In other words, the resistive switching depends on the right amount of oxygen vacancies in the device. Typical IV curves of TiN/TaO$_x$/W devices with TaO$_x$ deposited at different oxygen pressures, i.e., different oxygen vacancies, are shown in the supplementary material as Fig. S5.

Note that after being annealed at 500 °C, the devices were non-switchable due to the oxidation of the TaO$_x$ as well as the TiN bottom electrode, which is supported by the electrical measurement in Fig. 5 showing that the samples are insulating. This will be discussed in detail in the following paragraph.

Based on the XRD analysis (supplementary material, Fig. S6), up to 400 °C, the TaO$_x$ films were all amorphous, as indicated also with the grazing incidence x-ray diffraction (GIXD) experiments [Figs. S6(b)–S6(d)]. For annealing temperature above 400 °C, the amorphous TaO$_x$ crystallizes into a low-temperature β-phase at elevated temperatures between 500 °C to 700 °C.[13,18,19] The ordering process of the amorphous TaO$_x$ induced by thermal annealing is a slow process and hardly gets completed even at 700 °C.

B. The effect of electrodes and interfaces

Another source of the possible absence of resistive switching is the degradation of the electrodes during annealing. Besides the oxidation process of TaO$_x$, we also observe an indication of oxidation of the TiN electrode materials, i.e., from the transport measurements. After the annealing process (on samples similar to the one shown in Fig. 3), the resistivity of both the TiN bottom electrode layer and the W top electrode layer was tested using a four-probe van der Pauw configuration. The four-probe test was
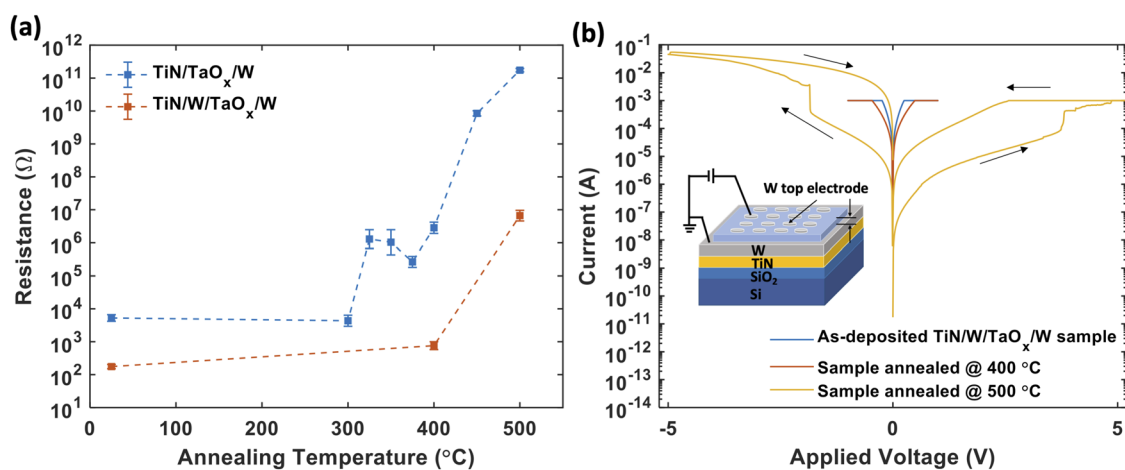

FIG. 6. (a) Resistance change of the TiN/TaO$_x$/W and TiN/W/TaO$_x$/W structured devices after the annealing process. (b) Typical IV curves for TiN/W/TaO$_x$/W structured devices.

carried out on the TiN layer of the devices, and on a new set of samples only consisting of bare W electrode. All tests were carried out at room temperature after the annealing process. The resistivity of the TiN layers shows an increase from 320 ± 19 $\mu\Omega$ cm

without any post-annealing process to 592 ± 61 $\mu\Omega$ cm after being annealed at $400\,^\circ$C. As the annealing temperatures increased above $400\,^\circ$C, the TiN layer became very insulating with a resistivity above the detection limit of our equipment (Fig. 5). On the other hand, the W layer kept a stable resistivity even after being annealed at $500\,^\circ$C.

In addition to the stoichiometry of the TaO$_x$ layer, one need also to ensure the right choice of the electrode combination, which is also a crucial factor for the resistive switching. By inserting a layer of W between the TiN and the TaO$_x$ (Si/SiO$_2$/TiN/W/TaO$_x$/W), as a "blocking" layer for oxygen, the resistance increased from 10^2 Ω to 10^7 Ω, see Fig. 6(a). However, no resistive switching was observed in these samples [Fig. 6(b)]. The devices showed an Ohmic *IV* relationship for the annealing temperature up to $400\,^\circ$C. Devices after being annealed at $500\,^\circ$C showed a forming/SET process but cannot be switched back to the high resistance state at the negative voltage side.

In order to understand the influence of annealing on the interface profiles, detailed STEM investigations were carried out on similar TiN/TaO$_x$/W samples (Fig. 3). Figures 7(a)–7(c) show STEM-HAADF images of the layered structure overlapped by the EDX scans. From STEM-EDX chemical investigations, it is clear that the out-of-plane elemental intermixing at both interfaces, TiN/TaO$_x$ and TaO$_x$/W, is present. The as-fabricated sample [Fig. 7(a)] shows no indication of clear intermixing, although there might be intermixing only at a very narrow interval close to the interface ($\sim$5 nm). For sample annealed at $325\,^\circ$C [Fig. 7(b)], the STEM EDX indicates that there is a diffusion of Ta into the W layer, while the W does not seem to diffuse into the TaO$_x$ layer (see also Fig. S7). After annealing at $500\,^\circ$C [Fig. 7(c)], we observe the diffusion of W into the TaO$_x$ as well as the diffusion of Ta into the W layer. Additionally, we have observed a diffusion of both Ta and O into the TiN layer. This supports our XPS and the electrical measurements indicating that the TiN is probably partially oxidized at $500\,^\circ$C.

IV. CONCLUSION

In this work, we were able to trigger the resistive switching in TiN/TaO$_x$/W devices by applying a post-annealing procedure. We identify three different temperature regimes.

- *T* $\leq$ **300** $^\circ$**C**: The devices are thermally stable when exposed to annealing in air up to $300\,^\circ$C for 4 h. With the given deposition parameters used for the TaO$_x$ deposition, no resistive switching was observed at room temperature.

- **300** $^\circ$**C** < *T* $\leq$ **400** $^\circ$**C**: The devices showed resistive switching after annealing within this temperature window. As indicated by the XPS depth profiling, in this temperature range, the TaO$_x$ layer reduces while the TiN is oxidized. In this temperature range, both the non-stoichiometry of TaO$_x$ and oxidation/reduction at the TaO$_x$/electrode interface played an essential role in triggering resistive switching.

- *T* > **400** $^\circ$**C**: We observed insulating films. This happened due to the oxidization of the TiN bottom electrode and the shift of the TaO$_x$ to the more stoichiometric composition.
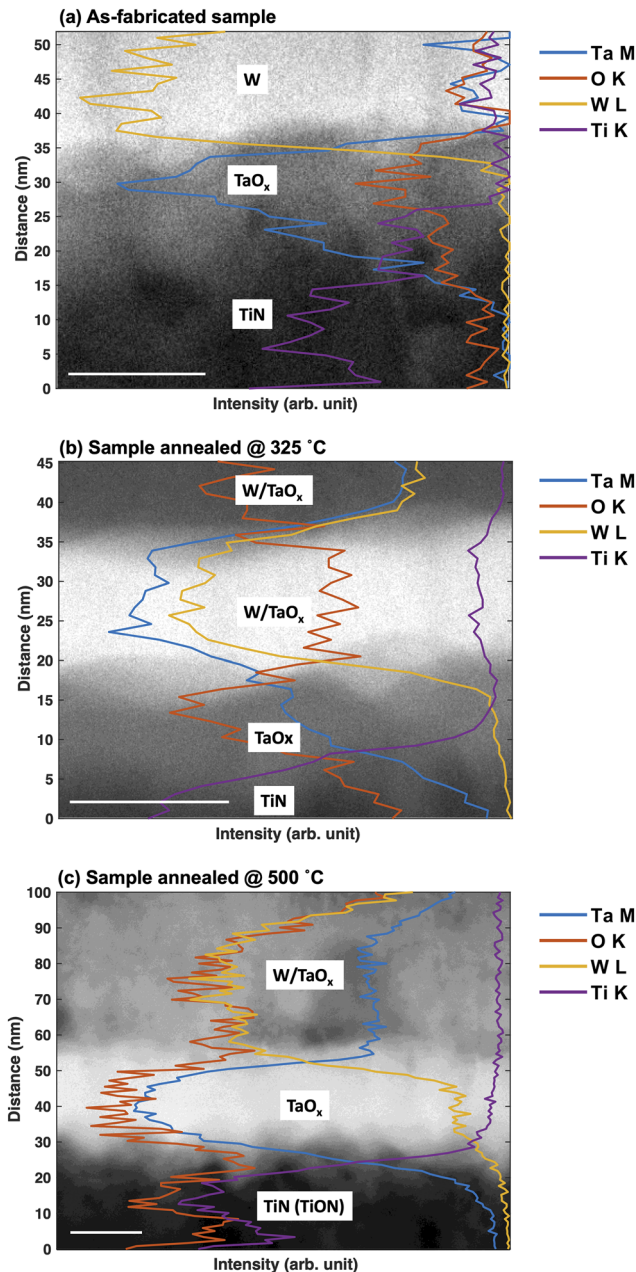

FIG. 7. STEM of TiN/TaO$_x$/W annealed under different conditions. The STEM-HAADF images are overlapped with the EDX line scans of (a) an as-fabricated device, (b) a device annealed at $325\,^\circ$C, and (c) a device annealed at $500\,^\circ$C. The elemental profiles are obtained using Ta M (blue), O K (orange), W L (yellow), and Ti K (purple) x-ray emission lines. The scale bars in (a)–(c) correspond to 20 nm. For the EDX line profiles, zero intensity is at the right side of the figure.

We have shown that post-annealing can enable resistive switching and allow studying the switching behavior in samples, which otherwise did not show resistive switching. Annealing can be a simple yet powerful method for triggering the resistive switching. By post-annealing the devices in a temperature range between 325 °C and 400 °C, the initial resistances of the $TiN/TaO_x/W$ structured devices increased from 10^3 Ω to 10^6 Ω resulting in the resistive switching. The temperature range observed in these experiments related to the stability of the electrodes and the active layer. Both the stoichiometric TaO_x layer and the TiN/TaO_x interface or the TiN electrode played an important role in the emergence of resistive switching behavior.

SUPPLEMENTARY MATERIAL

See the supplementary material for more information about the electrical test set-ups, the typical *I-V* curves and resistances of switchable devices, the XPS fitting details, the XRD spectra of TaO_x materials, and the supplementary information about EDX elemental profile.

ACKNOWLEDGMENTS

DATA AVAILABILITY

The data that support the findings of this study are available from the corresponding author upon reasonable request.

REFERENCES

[1] C.-W. Hsu, I.-T. Wang, C.-L. Lo, M. Chiang, W. Jang, C.-H. Lin, and T.-H. Hou, "Self-rectifying bipolar TaO_x/TiO_2 RRAM with superior endurance over 10^{12} cycles for 3D high-density storage-class memory," in *2013 Symposium on VLSI Circuits, Kyoto, Japan, 11-13 June 2013* (IEEE, Piscataway, NJ, 2013), pp. T166–T167, https://ieeexplore.ieee.org/abstract/document/6576643.

[2] A. C. Torrezan, J. P. Strachan, G. Medeiros-Ribeiro, and R. S. Williams, Nanotechnology **22**, 485203 (2011).

[3] S. P. Garg, N. Krishnamurthy, A. Awasthi, and M. Venkatraman, J. Phase Equilib. **17**, 63 (1996).

[4] Y. Li, S. Sanna, K. Norrman, D. V. Christensen, C. S. Pedersen, J. M. G. Lastra, M. L. Traulsen, V. Esposito, and N. Pryds, Appl. Surf. Sci. **470**, 1071 (2019).

[5] S. U. Sharath, M. J. Joseph, S. Vogel, E. Hildebrandt, P. Komissinskiy, J. Kurian, T. Schroeder, and L. Alff, Appl. Phys. Lett. **109**, 173503 (2016).

[6] H. Jeon, J. Park, W. Jang, H. Kim, C. Kang, H. Song, H. Kim, H. Seo, and H. Jeon, Phys. Status Solidi Appl. Mater. Sci. **211**, 2189 (2014).

[7] M. T. Brumbach, P. R. Mickel, A. J. Lohn, A. J. Mirabal, M. A. Kalan, J. E. Stevens, and M. J. Marinella, J. Vac. Sci. Technol., A **32**, 051403 (2014).

[8] J. Hong, W. Jang, H. Song, C. Kang, and H. Jeon, J. Korean Phys. Soc. **66**, 721 (2015).

[9] C. Chen, C. Song, J. Yang, F. Zeng, and F. Pan, Appl. Phys. Lett. **100**, 253509 (2012).

[10] L. Goux, J. Y. Kim, B. Magyari-Kope, Y. Nishi, A. Redolfi, and M. Jurczak, J. Appl. Phys. **117**, 124501 (2015).

[11] P. S. Dobal, R. S. Katiyar, Y. Jiang, R. Guo, and A. S. Bhalla, J. Raman Spectrosc. **31**, 1061 (2000).

[12] S. Lagergren and A. Magnéli, Acta Chem. Scand. **6**, 444 (1952).

[13] C. Joseph, P. Bourson, and M. D. Fontana, J. Raman Spectrosc. **43**, 1146 (2012).

[14] D. V. Christensen, M. von Soosten, F. Trier, T. S. Jespersen, A. Smith, Y. Chen, and N. Pryds, Adv. Electron. Mater. **3**, 1700026 (2017).

[15] L. Zhang, S. Member, R. Huang, S. Member, M. Zhu, and S. Qin, IEEE Electron Device Lett. **31**, 966 (2010).

[16] Y. Jiang, C. C. Tan, M. H. Li, Z. Fang, B. B. Weng, W. He, and V. Y.-Q. Zhuo, ECS J. Solid State Sci. Technol. **4**, N137 (2015).

[17] H.-Y. Chen and F.-H. Lu, J. Vac. Sci. Technol., A **23**, 1006 (2005).

[18] C. Chaneliere, J. L. Autran, R. A. B. Devine, and B. Balland, Mater. Sci. Eng. R Rep. **22**, 269 (1998).

[19] F.-C. Chiu, J.-J. Wang, J. Y. Lee, and S. C. Wu, J. Appl. Phys. **81**, 6911 (1997).